IEEE Access
Multidisciplinary | Rapid Review | Open Access Journal

Received November 26, 2020, accepted December 29, 2020, date of publication January 20, 2021, date of current version June 10, 2021.

Digital Object Identifier 10.1109/ACCESS.2021.3053117

An Event-Triggered Low-Cost Tactile Perception System for Social Robot's Whole Body Interaction

SHENGZHAO LIN[1], JIONGLONG SU[2], SIFAN SONG[2], AND JIAMING ZHANG[1,3]

[1]Institute of Robotics and Intelligent Manufacturing, The Chinese University of Hong Kong, Shenzhen 518172, China
[2]Department of Mathematical Sciences, Xi'an Jiaotong-Liverpool University, Suzhou 215123, China
[3]Shenzhen Institute of Artificial Intelligence and Robotics for Society, Shenzhen 518129, China

Corresponding author: Jiaming Zhang (zhangjiaming@cuhk.edu.cn)

This work was supported in part by the Shenzhen Science and Technology Innovation Commission, China, under Grant JCYJ20170410172100520, and in part by the Guangdong Basic and Applied Basic Research Foundation, China, under Grant 2019A1515110510.

ABSTRACT The social interaction is one of the necessary skills for social robots to better integrate into human society. However, current social robots interact mainly through audio and visual means with little reliance on haptic interaction. There still exist many obstacles for social robots to interact through touch: 1) the complex manufacturing process of the tactile sensor array is the main obstacle to lowering the cost of production; 2) the haptic interaction mode is complex and diverse. There are no social robot interaction standards and data sets for tactile interactive behavior in the public domain. In view of this, our research looks into the following aspects of tactile perception system: 1) Development of low-cost tactile sensor array, including sensor principle, simulation, manufacture, front-end electronics, examination, then applied to the social robot's whole body; 2) Establishment of the tactile interactive model and an event-triggered perception model in a social interactive application for the social robot, then design preprocessing and classification algorithm. In this research, we use k-nearest neighbors, tree, support vector machine and other classification algorithms to classify touch behaviors into six different classes. In particular, the cosine k-nearest neighbors and quadratic support vector machine achieve an overall mean accuracy rate of more than 68%, with an individual accuracy rate of more than 80%. In short, our research provides new directions in achieving low-cost intelligent touch interaction for social robots in a real environment. The low-cost tactile sensor array solution and interactive models are expected to be applied to social robots on a large scale.

INDEX TERMS Tactile sensor array, touch behavior, event trigger, tactile perception, machine learning.

I. INTRODUCTION

The human skin is the largest organ in the human body. It may perceive temperature, pressure, abrasion, texture and other complex information. Furthermore, it may, based on skin-to-skin touch, facilitate interaction, and affection, e.g., hugging, caressing and hand-shaking. Emotional contact plays a fundamental part in human relationship development, interpersonal communication and emotional support [1]–[5]. There is sustained interest to replicate the functionality of the human skin on social robots. Robots endowed with the sense of touch may find diverse applications in augmented reality, mixed reality, telemedicine, health surveillance, smart wear, machine interaction and others [6], [7]. Especially, with the intensification of global aging, service-oriented companion robots with social interaction functions and skills will receive more and more attention. Currently, research is primarily focuse on vision (facial expression, expression in eyes, hand gestures, postures, attention), audio (natural language, voice commands) [8]–[10], the combination of vision and audio [11], psychocardiogram of human-robot interactions [12], and brain-machine interface for human-robot interaction [13]. Apart from those, Vengadesh, A. *et al.* achieved the interaction between cleaning robots and human based on the color of light [14]. Although the research on touch-based interaction has shown to be effective in machine interaction and telemedicine [15]–[17], it has yet received widespread attention. The tactile perception of social interactive robots can obtain a more efficient interaction, especially in virtual media consumption or emotional remote

The associate editor coordinating the review of this manuscript and approving it for publication was Ze Ji.

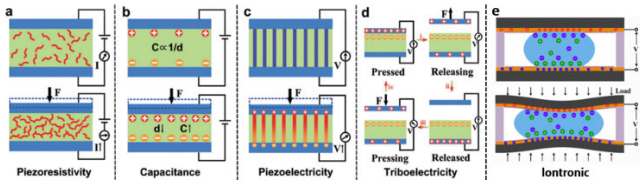

FIGURE 1. Common tactile sensing mechanisms: Piezoresistivity, capacitance, piezoelectricity, triboelectricity and iontronic.

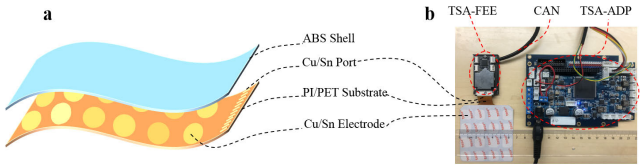

FIGURE 2. Flexible TSA structure (a) and FEE module, ADP module (b). The TSAs are assembled on the inner surface of the ABS shell of the social robot.

companionship [2]. Moreover, it also has unique advantages over traditional interaction methods (e.g., visual-based). For example, tactile perception can also obtain information on the stiffness, roughness, hardness, texture, etc. of the object being touched [18].

The main tactile sensing principles currently used are [19]–[27]: Piezoresistive Type, Piezoelectric Type, Capacitive Type, Triboelectric Type, Iontronic Type, Electromagnetic Type, e.g., Refer to Fig 1 for a diagrammatic description of the common mechanisms of tactile sensors. To increase the sensitivity of the sensors, most of the work in this domain is focused on the design and development of tactile sensors based on highly complex processing and novel materials. The common practice is to resort to the use of new materials and micropatterned structures [28]. However, the preparation of materials and the manufacture of sensors are particularly sophisticated, unstable and very costly [29]. As a result, large-area sensor arrays are not mass-produced and still in the laboratory exploration stage. This limits their large-scale application in tactile interaction for social robots.

In terms of human-robot interaction (HRI) applications, compared to the more common multi-layer complex structure, Sohn, K. S. *et al.* adopted the single-layered piezoresistive MVCNT-PDMS composite film to achieve very simple macroscale e-skin neither with nanoscale dimensions nor macro-patterns [30]. Correll used FPC at 10.8 $\times$ 10.8 cm^2 to construct 64 sensor arrays based on the principle of infrared reflection, and carried out classification of six types of touch gestures [31]. Lukowicz *et al.* carried out the production of textile fiber tactile sensors and their application to the classification of limited emotional touch gestures [32]. Do *et al.* researched different touch gestures and how they may be mapped to different emotional states [33]. MacLean used the sense of touch on tactile creature and their expected response to explore how human beings communicate emotions. He used nine commonly used touch gestures and introduced the touch dictionary [34]. There is also research on the use of smartphone screens to collect interactive data [35], and to predict cognitive states [36]. A more prominent report is on the iCub robot developed by the Italian technological research institute [37]–[39], which uses a low-cost solution. Shimoga in his research pointed out that hand gestures at relatively low speed while passing through large (hand) area does not require the presence of highly precise pressure level. Hence, low-tech method may cater to the applications in human-robot social interaction [40]. This provides a new idea in the applications of tactile sensing. Tactile perception applications, which are based on tactile sensing, are still in their infancy, e.g., machine learning-based intelligent tactile perception [41]. Naya *et al.* applied k-nearest neighbors (KNN) principles on pet-like robot tactile interface to classify touch modality. Gastaldo *et al.* used support vector machine (SVM) to process tactile mode information [42], [43].

The development of robot tactile perception system (TPS) is a systems engineering, and there are many challenges [42] in materials, electronics, telecommunications, signals processing, pattern recognition, etc. The main challenge lies in the high cost of tactile sensing array, complex manufacturing process, as well as the fact that the research is still ongoing, and a number of problems are still unresolved, e.g., unit consistency problem of the array device, modular excitation problem, and signal crosstalk problem [16]. Due to the complexity of tactile interaction modeling, it is rare to find research reporting on the standard model of touch behavior in a real interactive environment for social robots.

To Summarize, the current constraint on the general applications of tactile sensing array is mainly due to the relative complications in the manufacturing process of sensing array, which happens to be in the development stage. There is no tactile interaction model that satisfies the real social interaction environment, which refers to the interaction between the two parties without touch time and area constraints through various interaction modes with appropriate touch intensity. In the process of real social interaction, the interaction is not limited in time. Moreover, this interaction with limited time has weak robustness and reduces the actual tactile interaction applications [32]. As such, this paper looks into the research on low-cost tactile sensing arrays, related front-end electronics (FEE) modules, touch behavior as well as perceptual algorithms and modeling for breakthroughs in social robot interactions.

The novelty of this paper is two-fold. First, the low-cost tactile sensor array (TSA) on social interaction robots is produced with acrylonitrile butadiene styrene (ABS) shell. Second, we construct six models of touch interaction behavior from a real social interaction application; the use of a single touch event to depict the basic characteristics of touch behavior and for carrying out the perceptual classification.

The key contribution of this paper is three-fold. First, we propose a low-cost tactile sensing array that may be manufactured for a social robot whole body with ABS shell. We also carry out experiments to verify the feasibility of a low-cost process in social interaction robots. Second, we develop a set of FEE software and hardware modules. Third, we construct

event-based six touch interaction behavior models from a real social interaction environment without assumptions of fixed touch time and interactive objects. Furthermore, we carry out perceptual modeling and classification on these models, enhancing the robustness and adaptability of the social interaction system.

The rest of this paper is organized as follows. Section II introduces the development of tactile sensors, including sensing principles, sensor array modeling simulation, FEE, and sensor examination. The experiment setup is described in Section III. In Section IV, we discuss tactile perception classification, including feature model, touch behavior modalities, sensor array data preprocessing (ADP), and high-level abstract feature modeling. The results and discussion of our tactile perception system experiments are given in Section V. Finally, a summary of our research work and future work are concluded in Section VI.

II. TACTILE SENSOR HARDWARE

A. PRINCIPLE

Capacitive sensing is one of the most commonly utilized principles in robotic tactile sensing. It is attractive to researchers due to its high sensitivity and high resolution [30], [44], [45]. The TSAs are designed by the principle that the overall capacitance is changed by the touch pressure of the plate capacitor resulting in different spacing, dielectric and effective areas between two polar plates. The formula is written as,

$$C = \varepsilon \frac{A}{d} \tag{1}$$

where ε represents dielectric constant, A is the effective overlapping area between two conductive plates, and d is the distance between the two plates. The pressure applied to the sensor is measured by the change of A and d. In this study, the two capacitor electrode plates are composed of a body capacitor and a flexible plate. The electrode arrays are produced by the commercialized flexible printed circuit (FPC) process, capacitor electrode plates are constructed by a combination of polyimide (PI) and copper-tin materials.

B. SIMULATION

In order to understand the relative change relationship of self-capacitance and mutual-capacitance when a touch occurs, facilitate the FEE array signal readout design, according to the symmetry of array structure, the influence of model complexity and computing performance, the TSA simulation uses a 2×2 array for analysis, utilizes boundary element method [46] and physical field interface for modeling, and uses steady-state source for extracting lumped parameter arrays only with surface meshing. The movement of human finger or palm models are utilized to research the principle of capacitive position sensing. The shifting of the mesh is realized by applying the interface of a deformed geometric physical field, which simulates the approach of human fingers or palms [47]–[50]. Two structural models are applied in this paper. First, the testing object is oriented towards the center of the array and its area is equal to the area of this 2×2 array. Second, the testing object is oriented towards the center of one contact of the array and its area is equal to the area of this contact. These two structures are shown in Fig. 3. Since the absolute capacitance of electrodes may drift for long periods of time, it is more accurate to measure the relative change of the capacitance between electrodes during the post array signal detection, as shown by the black curve in (b). This method is also used for the embedded FEE.

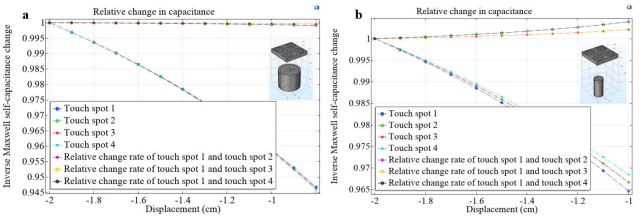

FIGURE 3. Self-capacitance and mutual-capacitance simulation of TSA, the TSAs are modeled using a 2 × 2 array. The responses of test objects progressively closing to a single contact and multiple contacts are simulated. (a) The area of the test object is equal to the area of four array terminals; There is no relatively change because the change is uniform when the object is progressively closing to the array terminals; (b) The area of the test object is equal to the area of one terminal; When the test object is progressively closing to the center of one array, the four array terminals have a large relative change. In (a) and (b), it is notable that the y-axes represent the change of self-capacitance and x-axes represent the distance.

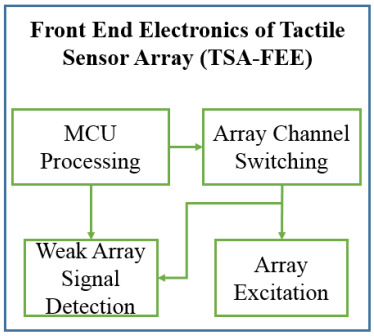

FIGURE 4. The structure of the FEE of TSA.

C. FEE MODULE

The architecture of FEE of TSA is shown in Fig. 4, which is responsible for array excitation and signal detection. We select low-cost and small encapsulated STM32F046 as the core processing unit of MCU. The MCU is responsible for not only signal excitation and detection of the array drive detection module but also the real-time switching controlled by the array channel switching module in terms of specific scanning strategies. The integrated capacitive digital conversion (CDC) chip of FDC2114 @TI is applied to the array drive detection module. The array drive detection front-end adopts an integrated anti-interference design to meet different application requirements, such as robots with limited internal space.

The completed TSAs are a passive component. By LC oscillatory excitation, it monitors the parameters of touch

behaviors, such as touch intensity, touch time, touch direction, touch area, etc. The capacitance changes when the tactile sensor array receives touch behaviors, resulting in the change of oscillation frequency. When the weak frequency change is detected by the FEE, corresponding digital values are computed by frequency digital conversion for back-end transmission and processing.

$$C_{SENSORx} + C = \frac{2^{28^2}}{L * (2\pi * 2 * f_{REFx} * DATAx)^2} \quad (2)$$

where C is the parasitic capacitance, f_{REFx} is the excitation frequency, L is the fixed inductance, $DATAx$ is the result of CDC. Based on this principle, the FEE readout circuit is built, consisting of a CAN communication circuit, a multi-channel scanning circuit and an oscillation excitation/detection circuit. MCU is applied for the unified scheduling of each circuit module. The relative change of the simulation of measurement array units is used to suppress the long-term drift of the sensing capacitance. This testing strategy is utilized to screen and filter array signals, reducing the negative effects caused by the long-term drift of the signals. Since the CDC chip only has the ability to drive 4 channels simultaneously, it is expanded to a 4 × 8 array by employing an external 4 × 8 multi-channel switching chip which is encoded to 2 × 4 × 4 channels. This configuration achieves a balance between frame rate and channel capacity.

D. EXAMINATION

In this study, the basic sheet of TSAs is composed of 16 touch points with a total area of 25 cm^2. Each contact has a diameter of 5 mm and the distance between adjacent centers of the contacts is 7mm. The test platform is the pressure tester (model ZQ-21A-2) of Dongguan City ZHIQU Precision Instruments Co. The TSA-FEE module has the frame rate of 8 Hz, 32 (2 × 16) channels, and 12 bits resolution per channel and the ability of single-ended (2 × 4 × 4 channels) and difference (4 × 4 channels) drive/detection with 250 pF detection range, 5 fF sensitivity, and CAN (1 Mbps) communication. It has the interface of FFC 16 pins, the power supply of 5 Vdc / 0.03 Amax and the geometric size of 24 mm × 45 mm, as shown in Fig. 2 (right). The test results are demonstrated in Fig. 5. Table 1 shows a comparison with the publicly reported iCub robotic tactile arrays at the Italian Institute of Technology.

III. ASSEMBLY AND EXPERIMENT SETUP

The TPS of social robot architecture and communication architecture is shown in Fig. 6 in this paper. The top layer consists of a PC computing endpoint layer and data storage, and it is responsible for not only handling the high-throughput concurrent data processing and storage tasks of the lower layer endpoints, but also responding to requirements of the lower layer nodes in real-time. The machine learning classification algorithm is implemented at this layer node. The connection between the top layer and the middle layer is connected by RS485 fieldbus. The middle layer is composed

TABLE 1. The comparison between the tactile sensor array designed in this paper and a published one.

Sensing Mode	Minimum Detection Limit	Maximum Pressure	Sensitivity	Linearity	Spatial Resolution	Application Examples
Capacitance	2-3kPa (3–4kPa)	180kPa (50kPa)	/	/	5 mm (3 mm)	iCub skin [38]
Capacitance	0.1kPa	30kPa	0.15 $pF{\cdot}kPa^{-1}{\cdot}cm^{-2}$	94%	5 mm	our research

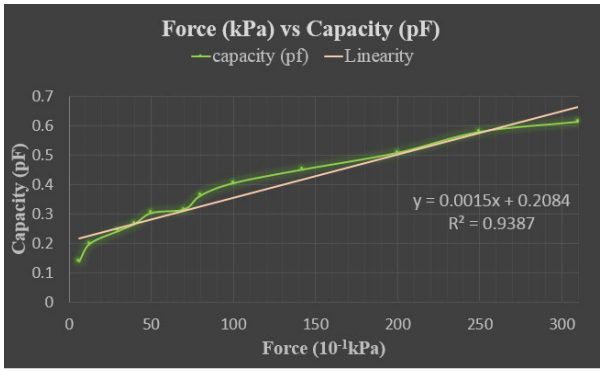

FIGURE 5. Testing curves of the tactile sensor arrays, with linearity R2 ≥ 94%, dynamic range 0.1kPa – 30kPa, sensitivity 0.15 pF·kPa-1·cm-2.

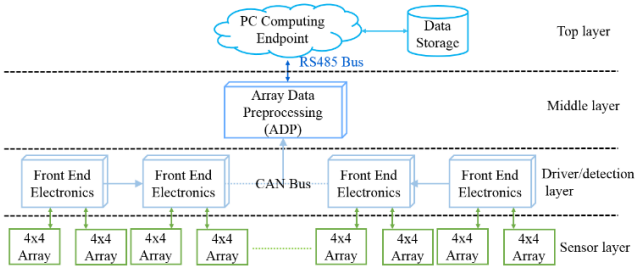

FIGURE 6. The architecture of TPS for social robot which equipped with whole body TSA-FEE.

of tactile ADP computing node, which is responsible for extracting and screening high-throughput data. The middle layer and the array drive/detection layer are connected via a CAN field serial bus. The array drive/detection layer consists of 21 FEE modules, each FEE mounts two basic sheets of TSAs. The tactile array data under different touch modalities are collected by FEE and uploaded to the ADP module through the CAN bus. Subsequently, the ADP module transmits the preprocessed tactile array data to the PC computing node through the RS485 bus.

The TSAs and FEEs are mounted on the inner surface of the ABS shell of the social robot. The assembly positions are distributed on the top of the robot's head, left and right cheeks, back of the head and forehead, left and right arms and thighs, and they are coded one by one, as shown in Fig. 7. Since the shell material of the social robot is ABS with a high elastic modulus, the touch intensity information becomes undesirable when using this installation method for suppleness and

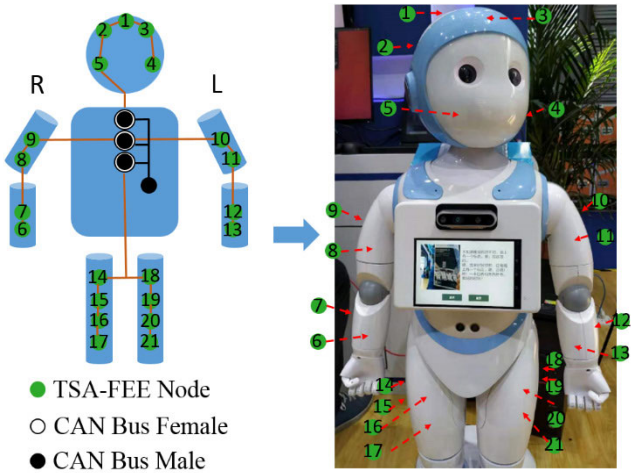

FIGURE 7. The assembly scheme of TSA-FEE of social robot. CAN bus is connected by a star network.

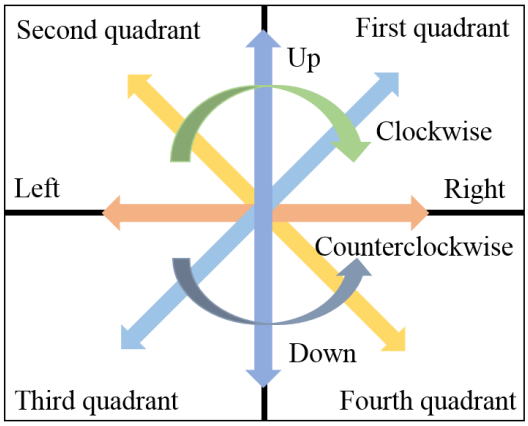

FIGURE 8. The touch direction is described by four quadrants and ten directions, namely, clockwise, counterclockwise, from left to right, from right to left, from up to down, from down to up, from upper left to lower right, from lower right to upper left, from lower left to upper right and from upper right to lower left.

TABLE 2. Descriptions of touch behaviors and corresponding mapping values.

Touch Behaviors	Descriptions	Mapping Values
Random Momentary Tapping	Random momentary tapping with a finger or the palm of a hand; the "momentary" represents a single touch event with a very short duration.	T1
Random Slow Sliding	Random momentary tapping with a finger or the palm of a hand; the "slow" represents a single touch event with a longer duration.	T2
Finger Sliding	Sliding with finger in any direction; the duration is faster than a slow sliding.	T3
Random Finger Poking	Random poking with a single finger on tactile arrays.	T4
Palm Momentary Tapping	Random momentary tapping with the palm of a hand; the "momentary" represents a single touch event with a very short duration.	T5
Palm Momentary Sliding	Sliding with the palm of a hand in any direction; the "momentary" represents a single touch event with a very short duration.	T6

beauty. In summary, the touch features used in this paper consist of 4 categories, namely touch time, area, direction and location. The baud rate of the single array drive detection front-end is $8\times32\times12 = 3072$ bps, so the total baud rate is 64.512 Kbps. A lot of noise information is mixed in these raw data and increases the burden of communication bandwidth. In this study, we utilize the IIR filtering algorithm which is similar to the moving average filter, except that the previous data is not stored.

$$Avg\,[i] = \frac{(Avg\,[i-1]\times N) - Avg\,[i-1] + val[i]}{N} \quad (3)$$

where N is the power of 2, and $val[i]$ represents the value of the current moment.

During the experiment, several touch modalities were predefined according to the touch interaction gestures commonly used in daily life as shown in Table 2, in which we select general touch modalities to avoid extreme situations. The touch direction is pre-defined for 10 types of touch directions as shown in Fig. 8. In order to improve the adaptability of the sensor array to different palm areas, large-scale array sensing was realized through array splicing in the experiment. In the tactile interaction experiment of this paper, a series of predefined touch behavior actions (Table 2) are performed on the TSAs through the palm or finger, such as pressing and touching, and then the corresponding touch behavior data is collected and preprocessed to extract the touch time, area, direction and location. The tester can touch the whole body of the social robot equipped with the touch sensor array (Fig 7) for any length of time, and the palm area of the tester is not strictly required. In order to simplify the model, only the tester can use one-handed operation in a single touch event. This is because modeling with multiple hands is complicated. The vector group $X = \bar{x}_j^i, i = (1, 2, 3, 4), j = (1, 2, \cdots N)$ consists of these four features and samples (A total of 1,000 samples were collected in this experiment, divided into adult male and female groups, of which 500 samples were in the male group). The vector group is classified by classification algorithms such as KNN, SVM, and tree. See the description of each part for details.

IV. TACTILE PERCEPTION CALSSIFICATION

A. CHARACTERISITICS DESCRIPTION

Based on the assembly scheme of TSA of the social robot and the tactile interactive mode in a real social interaction environment, the tactile characteristics are categorized into four dimensions (time, direction, area and location). The details are shown in Table 3.

In the process of real social interaction, the interaction is not usually restricted with a time limit and the palm area of each tester is also different. Moreover, this interaction with limited time has low robustness and reduces the actual social tactile interaction applications [32]. Therefore, we introduce event-based single touch events to describe and test the touch behaviors of both sides in this study. Especially, the touch

TABLE 3. Four types of primary tactile characteristics.

Characteristics	Description
Time	Described by multiplying the time required to scan a frame by the number of frames contained in a single touch event.
Direction	Calculated by the movement direction of the centroid per frame in a single touch event.
Area	Calculated by extracting the touch area from a single touch event and counting the number of triggered array points.
Location	Distributed in various parts of the robot, as shown in Fig. 7

time is defined by the number of frames contained in a touch behavior. This strategy is different from those studies using the time limit interaction.

A single touch event is detected by analyzing whether there is touch data occurring in two consecutive frames. If there is touch data in frame n and no touch data in frame $n+1$, the frames before frame n are defined as a single touch event. Moreover, each characteristic dimension is extracted and collected based on this single touch event. Therefore, the touch time, area, direction (such as from left to right, from up and down), location and touch mode are then extracted.

The single-touch event is defined as: n is defined as the number of frames, i, j are defined as intra-frame positions, and the correlation coefficient of two consecutive frames is defined as,

$$Ccov^n = X^{n+1} - X^n, Ccov^n \in \begin{cases} 1 \\ 0 \\ -1 \end{cases} \tag{4}$$

where X^n represents the matrix composed of $x^n_{(i,j)}$. A single touch event is defined when as only $Ccov^n$ is triggered with an edge ($''0 \rightarrow 1''$ represents a single touch event occurred or $''0 \rightarrow -1''$ represents the end of a single touch event). If frame is not empty ($X^n \neq 0$), it is labeled as 1, otherwise, it is labeled as 0. For saving transmission bandwidth, only after a single touch event and preset trigger threshold for each channel are triggered simultaneously, the FEE transmits a combination of the filtered 12 bit tactile array data ($DATAx$, as shown in Equation 2) and -1/1 flag to ADP through the CAN star network.

The description of intra-frame features:

D1: Average of all contacts per frame;

D2: Maximum value of all contacts per frame;

D3: Standard deviation of all contacts per frame;

D4: Maximum distance from frame center in each frame;

$$\overline{D_x} = \frac{1}{N}\sum_{n=1}^{N} D_x(n) \tag{5}$$

$$std(D_x) = \sqrt{\frac{1}{N-1}\sum_{n=1}^{N}\left|D_x(n) - \overline{D_x}\right|^2} \tag{6}$$

where $x = 1, 2, 3, 4$, and N is the number of frames contained in a single touch event.

B. ARRAY DATA PREPROCESSING

Except that the touch time and touch location can be directly obtained from the TSA and FEE, the touch direction and touch area are high-level abstract features that can be obtained by preprocessing the original array data. The direction of a single touch event is estimated by a centroid algorithm (the touch direction definition is shown in Fig. 8). The centroid of a touch array per frame is computed by averaging the matrix formed by the coordinates of this touch location, as shown in the formula (7). Therefore, the movement of centroids between frames determines the direction and step length of this single touch.

$$(\bar{x_i}, \bar{y_i}) = \frac{\sum_{j=k_1}^{k_m}(x_j, y_j)}{m} \tag{7}$$

where k_m represents the coordinates of m touch locations per frame, and i represents the i^{th} frame of a single touch event.

The touch area is calculated by the summation of the Euclidean distance between non-zero touch locations and their corresponding centroids per frame. The formula is written as,

$$A = \sum_i \sqrt{\sum_{j=1}^{k_m}\left(x_j - x_{c_i}\right)^2 + \left(y_j - y_{c_i}\right)^2} \tag{8}$$

where $\left(x_{c_i}, y_{c_i}\right)$ represents the centroid of the touch location in i^{th} frame.

The characteristics of tactile arrays (time, direction, area and location) form four-dimensional vectors. These vectors further construct a $Nx4$ matrix based on the sample size, N. Due to the large amount of data in multi-channel tactile arrays, the corresponding matrix is also very large. Therefore, the data transmission, storage and feature extraction are extremely difficult and complicated. To address this problem, we use the principal component analysis (PCA) for dimension reduction. Fig. 9 shows the visualization of partial touch samples containing three touch characteristics (time, area and direction).

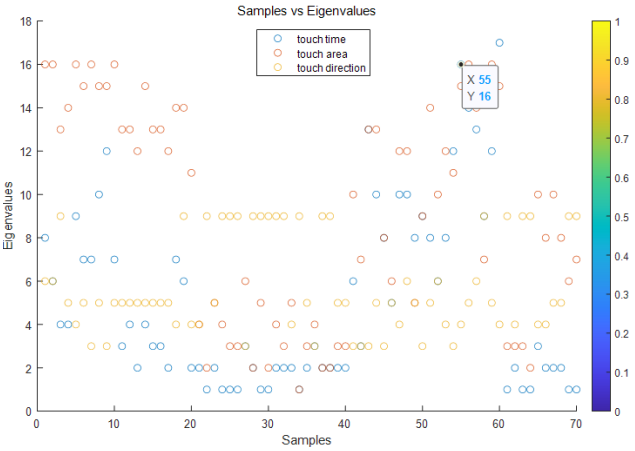

FIGURE 9. Visualization of partial touch samples containing three touch characteristics (time, area and direction), showing that the features are not linearly separable.

V. RESULTS AND DISCUSSIONS

A. PERCEPTUAL CLASSIFICATION

In practical modeling, touch behaviors are affected by the conditions of different experimenters. The combinatorial

TABLE 4. The results of 10 classification methods for six types of touch behaviors.

Classification Methods	Types					
	Random Momentary Tapping	Random Slow Sliding	Finger Sliding	Random Finger Poking	Palm Momentary Tapping	Palm Momentary Sliding
Medium Tree	57%	46%	50%	77%	70%	75%
Quadratic Discriminant	56%	50%	50%	77%	75%	55%
Gaussian Naïve Bayes	57%	56%	60%	82%	67%	60%
Kernel Naïve Bayes	60%	50%	56%	77%	70%	50%
Quadratic SVM	67%	55%	60%	75%	70%	83%
Cubic SVM	71%	56%	60%	73%	70%	63%
Medium Gaussian SVM	75%	50%	60%	79%	78%	67%
Cosine KNN	100%	50%	60%	67%	64%	71%
Weighted KNN	56%	57%	60%	70%	67%	56%
Subspace KNN	63%	73%	71%	78%	67%	50%

modeling of multiple touch methods will be more difficult. However, there is no internationally recognized standard, and the existing models are still not robust in a real social interaction application [32]. Due to the restriction of the AI algorithm interpretability [51]–[56], we use 10 classification methods, such as tree, linear discrimination, Bayesian, SVM, and KNN [57]–[59], to carry out the perceptual classification for the established models of touch behaviors and single touch events in this paper. The classification methods also combine PCA and K-fold cross-validation approaches where K is 7, N of KNN is 10 and the sample size is 1000. Table 4 and Fig. 10 give the classification results of 10 classification algorithms for six types of touch behaviors. They indicate that cosine KNN, weighted KNN and subspace KNN achieve the best performance on the results of random momentary tapping. Cosine KNN and quadratic SVM outperform other algorithms with overall mean accuracy rates of more than 68% and with individual recognition rates of more than 80%. For example, the recognition rate of quadratic SVM on palm momentary sliding reaches 83% and the rate of cosine KNN on the random momentary tapping reaches more than 95%. Although other algorithms perform better in the results of some individual touch behaviors, quadratic SVM and cosine KNN achieve better overall classification and recognition accuracies than others.

B. DISCUSSIONS

From the classification accuracies of 10 algorithms, it can be seen that the overall classification results are not very good

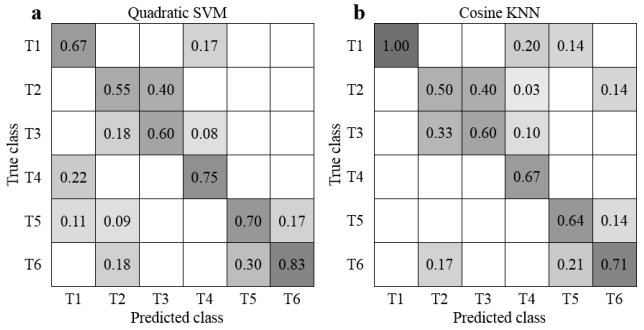

FIGURE 10. The confusion matrix of six touch behaviors using quadratic SVM (a) and cosine KNN (b), respectively.

(TABLE 4 and Fig 10). This is largely due to the selected model (including feature model, touch model and classification model). In order to simulate real social interaction applications as much as possible, we do not pre-specify the tester's touch time and the tester's palm area in feature modeling [32]. In addition, due to the way the TSAs are installed on the inner surface of the ABS shell of the social robot, touch intensity information cannot be obtained (Although it is very important). Furthermore, in terms of touch directions, only 10 directions are pre-defined, but in the testing process, the tester is not required to strictly follow the pre-defined touch directions for testing, all of which are to be as close as possible to real social interaction applications. To avoid some extreme touch modes during the test, we chose six touch modes, and the tester is required to strictly abide by the agreement.

Nevertheless, we observe that quadratic SVM and cosine KNN are superior to other algorithms on the overall performance of six touch behaviors [57]–[59]. This also indirectly verifies some of the conclusions obtained by previous researchers [42], [43]. This may be caused by the following reasons:

(1) The entire process of KNN algorithm is regarded as an optimization problem by optimizing the objective function through continuous iteration. The objective function of KNN is written as,

$$J = \sum_{j=1}^{k} \sum_{i=1}^{n} Dist(x_i, \mu_j) \tag{9}$$

The objective function shows that two factors (k-value and distance measure) have crucial effects on clustering results. For the distance-based clustering algorithms such as KNN, the distance measure is utilized throughout the algorithm.

$$Dist_{cos}(X, Y) = \frac{\sum_{i=1}^{d} x_i y_i}{\sqrt{\sum_{i=1}^{d} x_i^2} \sqrt{\sum_{i=1}^{d} y_i^2}} \tag{10}$$

As shown in the above formula, cosine distance reflects the similarity in terms of the cosine value between two vectors. It calculates the difference between two vectors in direction and is insensitive to absolute values (correcting for possible measure inconsistencies). At the same time, in the case of touch behavioral characteristics, especially touch direction,

the focus of data is on the directional information between feature points.

(2) Since the feature of touch samples is not linearly separable in the original space (as shown in Fig. 9), we apply SVM to achieve classification by transforming the data into a high-dimensional space using kernel functions. However, the curse of dimensionality can appear when the dimension number is excessively high. The touch behavior data does not present visual features, but its features are similar to those of text data. The recognition accuracies demonstrate that all SVM with kernel functions achieve good overall performance. Since the excessively high dimension of kernel functions may cause overfitting, the quadratic SVM outperforms other kinds of SVM in all six behaviors. However, the underlying reasons for the superior performance of quadratic SVM and cosine KNN on the overall classification results of the six touch behaviors are still a scientific problem for AI interpretability. Currently, black box testing is the most common approach to explore the performance of AI algorithms [51]–[56].

The results of touch behavior classification indicate that quadratic SVM and cosine KNN have great advantages in recognizing the above six types of touch behaviors. The mean recognition rates of these two algorithms are above 68%, and the individual recognition accuracies of some touch behavior types are more than 80%. In particular, the recognition rate of palm momentary sliding (quadratic SVM) is 83% and that of random momentary tapping (cosine KNN) is more than 95%.

VI. CONCLUSION AND FUTURE WORK

In this research, we look into the low-cost industrial development of tactile sensor arrays with the principle of capacitive sensing. The architecture of these arrays is designed, and its simulation is used to reveal the relative change of capacitance and guide the reading design of the FEE module. We develop customized FEE embedded software and hardware module and ADP module, install TSAs and FEEs to the whole body of a social robot wrapped in an ABS shell, design the TPS for social interaction robot, created several common social touch interaction models and four feature models, and use ML methods to classify them for testing the tactile interaction of social robots in a real social interaction environment. In terms of the tactile perceptual algorithms, the social touch interaction models and mathematical models are designed from the extraction of basic touch characteristics (time, area, direction, location). In order to simulate real social interaction applications as much as possible, we do not pre-specify the tester's touch time and the tester's palm area in feature modeling, all of which are to be as close as possible to real social interaction applications. The 10 algorithms including tree methods, SVM, and KNN are selected and tested using K-fold cross-validation. As a result, quadratic SVM and cosine KNN show superiority on the overall classification performance of six touch behaviors under the absence of key touch intensity information. They achieve average recognition rates of more than 68%, with individual recognition rates of more than 80%.

The currently developed low-cost TSAs are difficult to obtain more touch information, such as touch intensity, based on the capacitive principle and installation method, and not yet fully flexible and stretchable, which causes the failure to fit the social robot ABS shell well, resulting in a decrease in electric field intensity and sensitivity, and classification effect is not ideal. Furthermore, the TPS cannot achieve multi-functional and multi-parametric real-time perception. Furthermore, the result is obtained based on limited samples and machine learning algorithms. These perceptive algorithms have yet been combined with other technologies, such as visual and audio perceptions.

For future research, we could focus on four directions: (1) The research on flexibility, stretchability and versatility of low-cost tactile sensor arrays. For example, recognizing temperature and intensity (such as using strain sensing principles to monitor the deformation of an ABS shell) from tactile interactive behaviors. (2) Using small sample learning algorithms or increasing the number of samples to obtain more datasets. By collecting the touch patterns of children with autism using the rehabilitation robots, we can further verify the feasibility of the protocol. In addition, since some children with autism have weak cognitive abilities and simple touch interaction patterns, we can combine the professional diagnosis as a clinical trial of touch interaction for children with autism to determine whether robots with whole-body tactile perception interaction can improve the tactile interaction ability of these children. This approach may promote the use of robots with whole-body tactile perception interaction in the rehabilitation of children with autism. (3) Create a publicly available dataset of natural tactile features. This dataset has privacy protection and can satisfy the testing requirements of different tactile sensors and different sensing features in natural touch interaction scenarios. This is a $[N, M]$-dimensional dataset where N represents the number of samples and M is the number of sample features, such as the number of features corresponding to various gestures, the number of features corresponding to the combined interaction of multiple touch behaviors, and the number of features labeled with various touch emotions. (4) The research on multi-sensory technology, such as the combination of tactile, visual and audio perceptions, exploring the multi-view interaction behavior for achieving more intelligent machine interaction applications.

REFERENCES

[1] R. Andreasson, B. Alenljung, E. Billing, and R. Lowe, "Affective touch in human–robot interaction: Conveying emotion to the nao robot," *Int. J. Social Robot.*, vol. 10, no. 4, pp. 473–491, Sep. 2018.

[2] M. D. Cooney, S. Nishio, and H. Ishiguro, "Importance of touch for conveying affection in a multimodal interaction with a small humanoid robot," *Int. J. Humanoid Robot.*, vol. 12, no. 1, Mar. 2015, Art. no. 1550002.

[3] M. A. Eid and H. Al Osman, "Affective haptics: Current research and future directions," *IEEE Access*, vol. 4, pp. 26–40, 2016.

[4] R. S. Dahiya, G. Metta, M. Valle, and G. Sandini, "Tactile sensing—From humans to humanoids," *IEEE Trans. Robot.*, vol. 26, no. 1, pp. 1–20, Feb. 2010.

[5] M. J. Hertenstein, R. Holmes, M. McCullough, and D. Keltner, "The communication of emotion via touch," *Emotion*, vol. 9, no. 4, pp. 566–573, 2009.

[6] F. M. Petrini, M. Bumbasirevic, G. Valle, V. Ilic, P. Mijović, P. Čvančara, F. Barberi, N. Katic, D. Bortolotti, D. Andreu, K. Lechler, A. Lesic, S. Mazic, B. Mijović, D. Guiraud, T. Stieglitz, A. Alexandersson, S. Micera, and S. Raspopovic, "Sensory feedback restoration in leg amputees improves walking speed, metabolic cost and phantom pain," *Nature Med.*, vol. 25, no. 9, pp. 1356–1363, Sep. 2019.
[7] M. Park, B.-G. Bok, J.-H. Ahn, and M.-S. Kim, "Recent advances in tactile sensing technology," *Micromachines*, vol. 9, no. 7, p. 321, Jun. 2018.
[8] M. A. V. J. Muthugala and A. G. B. P. Jayasekara, "A review of service robots coping with uncertain information in natural language instructions," *IEEE Access*, vol. 6, pp. 12913–12928, 2018.
[9] P. Tsarouchi, S. Makris, and G. Chryssolouris, "Human–robot interaction review and challenges on task planning and programming," *Int. J. Comput. Integr. Manuf.*, vol. 29, no. 8, pp. 916–931, Aug. 2016.
[10] N. Mavridis, "A review of verbal and non-verbal human-robot interactive communication," *Robot. Auto. Syst.*, vol. 63, pp. 22–35, Jan. 2015.
[11] Z. Zeng, M. Pantic, G. I. Roisman, and T. S. Huang, "A survey of affect recognition methods: Audio, visual, and spontaneous expressions," *IEEE Trans. Pattern Anal. Mach. Intell.*, vol. 31, no. 1, pp. 39–58, Jan. 2009.
[12] K. R. Scherer, T. Bänziger, and E. Roesch Eds., *A Blueprint for Affective Computing: A Sourcebook and Manual*. Oxford, U.K.: Oxford Univ. Press, 2010.
[13] J. G. Makin, D. A. Moses, and E. F. Chang, "Machine translation of cortical activity to text with an encoder–decoder framework," *Nature Neurosci.*, vol. 23, pp. 1–8, Apr. 2020.
[14] M. V. J. Muthugala, A. Vengadesh, X. Wu, M. R. Elara, M. Iwase, L. Sun, and J. Hao, "Expressing attention requirement of a floor cleaning robot through interactive lights," *Autom. Construct.*, vol. 110, Feb. 2020, Art. no. 103015.
[15] T. L. Chen, C. H. King, A. L. Thomaz, and C. C. Kemp, "Touched by a robot: An investigation of subjective responses to robot-initiated touch," in *Proc. 6th ACM/IEEE Int. Conf. Hum.-Robot Interact. (HRI)*, Mar. 2011, pp. 457–464.
[16] C. Bartolozzi, L. Natale, F. Nori, and G. Metta, "Robots with a sense of touch," *Nature Mater.*, vol. 15, no. 9, p. 921, 2016.
[17] M. von Mohr, L. P. Kirsch, and A. Fotopoulou, "The soothing function of touch: Affective touch reduces feelings of social exclusion," *Sci. Rep.*, vol. 7, no. 1, 2017, Art. no. 13516.
[18] H. Liu, Y. Wu, F. Sun, and D. Guo, "Recent progress on tactile object recognition," *Int. J. Adv. Robotic Syst.*, vol. 14, no. 4, Jul. 2017, Art. no. 172988141771705.
[19] D. Silvera-Tawil, D. Rye, and M. Velonaki, "Artificial skin and tactile sensing for socially interactive robots: A review," *Robot. Auton. Syst.*, vol. 63, no. 3, pp. 230–243, Jan. 2015.
[20] S. Li, N. Pan, Z. Zhu, R. Li, B. Li, J. Chu, G. Li, Y. Chang, and T. Pan, "All-in-one iontronic sensing paper," *Adv. Funct. Mater.*, vol. 29, no. 11, Mar. 2019, Art. no. 1807343.
[21] X. Yu, Z. Xie, Y. Yu, J. Lee, A. Vazquez-Guardado, H. Luan, J. Ruban, X. Ning, A. Akhtar, D. Li, and B. Ji, "Skin-integrated wireless haptic interfaces for virtual and augmented reality," *Nature*, vol. 575, no. 7783, pp. 473–479, Nov. 2019.
[22] C. Wang, K. Xia, H. Wang, X. Liang, Z. Yin, and Y. Zhang, "Advanced carbon for flexible and wearable electronics," *Adv. Mater.*, vol. 31, no. 9, 2019, Art. no. 1801072.
[23] H. Yang, T. Xue, F. Li, W. Liu, and Y. Song, "Graphene: Diversified flexible 2D material for wearable vital signs monitoring," *Adv. Mater. Technol.*, vol. 4, no. 2, Dec. 2018, Art. no. 1800574.
[24] S. Chen, K. Jiang, Z. Lou, D. Chen, and G. Shen, "Recent developments in graphene-based tactile sensors and E-Skins," *Adv. Mater. Technol.*, vol. 3, no. 2, Feb. 2018, Art. no. 1700248.
[25] M. Jian, C. Wang, Q. Wang, H. Wang, K. Xia, Z. Yin, M. Zhang, X. Liang, X. Liang, and Y. Zhang, "Advanced carbon materials for flexible and wearable sensors," *Sci. China Mater.*, vol. 60, no. 11, pp. 1026–1062, 2017.
[26] N. Luo, Y. Huang, J. Liu, S.-C. Chen, C. P. Wong, and N. Zhao, "Hollow-structured graphene-silicone-composite-based piezoresistive sensors: Decoupled property tuning and bending reliability," *Adv. Mater.*, vol. 29, no. 40, Oct. 2017, Art. no. 1702675.
[27] Y. Wan, Y. Wang, and C. F. Guo, "Recent progresses on flexible tactile sensors," *Mater. Today Phys.*, vol. 1, pp. 61–73, Jun. 2017.
[28] S. C. B. Mannsfeld, B. C.-K. Tee, R. M. Stoltenberg, C. V. H.-H. Chen, S. Barman, B. V. O. Muir, A. N. Sokolov, C. Reese, and Z. Bao, "Highly sensitive flexible pressure sensors with microstructured rubber dielectric layers," *Nature Mater.*, vol. 9, no. 10, pp. 859–864, Oct. 2010.
[29] W. Peng and H. Wu, "Flexible and stretchable photonic sensors based on modulation of light transmission," *Adv. Opt. Mater.*, vol. 7, no. 12, Jun. 2019, Art. no. 1900329.
[30] K. S. Sohn, J. Chung, M. Y. Cho, S. Timilsina, W. B. Park, M. Pyo, N. Shin, K. Sohn, and J. S. Kim, "An extremely simple macroscale electronic skin realized by deep machine learning," *Sci. Rep.*, vol. 7, no. 1, pp. 1–10, 2017.
[31] D. Hughes, J. Lammie, and N. Correll, "A robotic skin for collision avoidance and affective touch recognition," *IEEE Robot. Autom. Lett.*, vol. 3, no. 3, pp. 1386–1393, Jul. 2018.
[32] B. Zhou, C. Altamirano, H. Zurian, S. Atefi, E. Billing, F. Martinez, and P. Lukowicz, "Textile pressure mapping sensor for emotional touch detection in human-robot interaction," *Sensors*, vol. 17, no. 11, p. 2585, Nov. 2017.
[33] H. Y. Joung and E. Y. L. Do, "Tactile hand gesture recognition through haptic feedback for affective online communication," in *Proc. Int. Conf. Universal Access Hum.-Comput. Interact.* Berlin, Germany: Springer, Jul. 2011, pp. 555–563.
[34] S. Yohanan and K. E. MacLean, "The role of affective touch in human-robot interaction: Human intent and expectations in touching the haptic creature," *Int. J. Social Robot.*, vol. 4, no. 2, pp. 163–180, Apr. 2012.
[35] M. Kim, H.-J. Kim, S.-J. Lee, and Y. Sang Choi, "A touch based affective user interface for smartphone," in *Proc. IEEE Int. Conf. Consum. Electron. (ICCE)*, Jan. 2013, pp. 606–607.
[36] P. Mock, P. Gerjets, M. Tibus, U. Trautwein, K. Möller, and W. Rosenstiel, "Using touchscreen interaction data to predict cognitive workload," in *Proc. 18th ACM Int. Conf. Multimodal Interact.*, Oct. 2016, pp. 349–356.
[37] L. Penco, N. Scianca, V. Modugno, L. Lanari, G. Oriolo, and S. Ivaldi, "A multimode teleoperation framework for humanoid loco-manipulation: An application for the iCub robot," *IEEE Robot. Autom. Mag.*, vol. 26, no. 4, pp. 73–82, Dec. 2019.
[38] G. Metta, G. Sandini, D. Vernon, L. Natale, and F. Nori, "The iCub humanoid robot: An open platform for research in embodied cognition," in *Proc. 8th Workshop Perform. Metrics Intell. Syst. (PerMIS)*, Aug. 2008, pp. 50–56.
[39] N. G. Tsagarakis, G. Metta, G. Sandini, D. Vernon, R. Beira, F. Becchi, L. Righetti, J. Santos-Victor, A. J. Ijspeert, M. C. Carrozza, and D. G. Caldwell, "ICub: The design and realization of an open humanoid platform for cognitive and neuroscience research," *Adv. Robot.*, vol. 21, no. 10, pp. 1151–1175, Jan. 2007.
[40] K. B. Shimoga, "Finger force and touch feedback issues in dexterous telemanipulation," in *Proc. 4th Annu. Conf. Intell. Robotic Syst. Space Explor.*, Sep. 1992, pp. 159–178.
[41] A. Ibrahim, P. Gastaldo, H. Chible, and M. Valle, "Real-time digital signal processing based on FPGAs for electronic skin implementation," *Sensors*, vol. 17, no. 3, p. 558, Mar. 2017.
[42] L. Zou, C. Ge, Z. Wang, E. Cretu, and X. Li, "Novel tactile sensor technology and smart tactile sensing systems: A review," *Sensors*, vol. 17, no. 11, p. 2653, Nov. 2017.
[43] A. Servati, L. Zou, Z. Wang, F. Ko, and P. Servati, "Novel flexible wearable sensor materials and signal processing for vital sign and human activity monitoring," *Sensors*, vol. 17, no. 7, p. 1622, Jul. 2017.
[44] Q. Zhang, Y. L. Wang, Y. Xia, P. F. Zhang, T. V. Kirk, and X. D. Chen, "Textile-only capacitive sensors for facile fabric integration without compromise of wearability," *Adv. Mater. Technol.*, vol. 4, no. 10, 2019, Art. no. 1900485.
[45] Y. Gu, T. Zhang, H. Chen, F. Wang, Y. Pu, C. Gao, and S. Li, "Mini review on flexible and wearable electronics for monitoring human health information," *Nanosc. Res. Lett.*, vol. 14, no. 1, pp. 1–15, Dec. 2019.
[46] M. Ayyildiz, M. Scaraggi, O. Sirin, C. Basdogan, and B. N. Persson, "Contact mechanics between the human finger and a touchscreen under electroadhesion," *Proc. Nat. Acad. Sci. USA*, vol. 115, no. 50, pp. 12668–12673, 2018.
[47] S. Maity, M. He, M. Nath, D. Das, B. Chatterjee, and S. Sen, "Bio-physical modeling, characterization, and optimization of electro-quasistatic human body communication," *IEEE Trans. Biomed. Eng.*, vol. 66, no. 6, pp. 1791–1802, Jun. 2019.
[48] X.-Q. Zhu, Y.-X. Guo, and W. Wu, "Investigation and modeling of capacitive human body communication," *IEEE Trans. Biomed. Circuits Syst.*, vol. 11, no. 2, pp. 474–482, Apr. 2017.
[49] Y. Xu, Z. Huang, S. Yang, Z. Wang, B. Yang, and Y. Li, "Modeling and characterization of capacitive coupling intrabody communication in an in-vehicle scenario," *Sensors*, vol. 19, no. 19, p. 4305, Oct. 2019.

[50] T. Grosse-Puppendahl, "Capacitive sensing and communication for ubiquitous interaction and environmental perception," Ph.D. dissertation, Dept. Comput. Sci., TU Darmstadt, Darmstadt, Germany, May 2015.
[51] W. Knight, "The dark secret at the heart of al," *Technol. Rev.*, vol. 120, no. 3, pp. 54–61, 2017.
[52] M. Edmonds, F. Gao, H. Liu, X. Xie, S. Qi, B. Rothrock, Y. Zhu, Y. N. Wu, H. Lu, and S.-C. Zhu, "A tale of two explanations: Enhancing human trust by explaining robot behavior," *Sci. Robot.*, vol. 4, no. 37, Dec. 2019, Art. no. eaay4663.
[53] F. Doshi-Velez and B. Kim, "Towards a rigorous science of interpretable machine learning," 2017, *arXiv:1702.08608*. [Online]. Available: http://arxiv.org/abs/1702.08608
[54] C. Molnar, G. Casalicchio, and B. Bischl, "Interpretable machine learning—A brief history, state-of-the-art and challenges," 2020, *arXiv:2010.09337*. [Online]. Available: http://arxiv.org/abs/2010.09337
[55] L. Breiman, "Statistical modeling: The two cultures," *Qual. Control Appl. Statist.*, vol. 48, no. 1, pp. 81–82, 2003.
[56] V. Nagarajan and J. Z. Kolter, "Uniform convergence may be unable to explain generalization in deep learning," in *Proc. Adv. Neural Inf. Process. Syst.*, 2019, pp. 11611–11622.
[57] M. Fernández-Delgado, E. Cernadas, S. Barro, and D. Amorim, "Do we need hundreds of classifiers to solve real world classification problems?" *J. Mach. Learn. Res.*, vol. 15, no. 1, pp. 3133–3181, 2014.
[58] R. Caruana, N. Karampatziakis, and A. Yessenalina, "An empirical evaluation of supervised learning in high dimensions," in *Proc. 25th Int. Conf. Mach. Learn. (ICML)*, 2008, pp. 96–103.
[59] G. Wang, T. Wang, H. Zheng, and B. Y. Zhao, "Man vs. machine: Practical adversarial detection of malicious crowdsourcing workers," in *Proc. 23rd USENIX Secur. Symp. (USENIX Security)*, 2014, pp. 239–254.

SHENGZHAO LIN received the Ph.D. degree in physical electronics from the University of Science and Technology of China, Hefei, Anhui, China, in June 2016. Since December 2017, he has been involved in Postdoctoral Research with the Institute of Robotics and Intelligent Manufacturing, The Chinese University of Hong Kong, Shenzhen, China, from March 2018 to January 2020, where he is currently an Associate Researcher with the Institute of Robotics and Intelligent Manufacturing. He joined the 26th Research Institute of China Electronics Technology Group, Chongqing, China, in July 2016. His research interests include mainly intelligent devices and intelligent terminal systems for intelligent robots.

JIONGLONG SU received the Ph.D. degree in statistics (Warwick) and the Ph.D. degree in automatic control and systems engineering (Sheffield). He worked with Warwick University, University College London, and Nazarbayev University, where he was the Maths Head. He is currently the Deputy Dean of the School of Artificial Intelligence and Advanced Computing, XJTLU Entrepreneur College (Taicang). His research interests include bioinformatics, artificial intelligence, and medical image processing.

SIFAN SONG received the B.S. degree from Xi'an Jiaotong-Liverpool University, China, in 2015, and the first M.S. degree in bioinformatics from the University of Edinburgh, in 2016, and the second M.S. degree in artificial intelligence from the University of Southampton, U.K., in 2019. He is currently pursuing the Ph.D. degree with the University of Liverpool based in Xi'an Jiaotong-Liverpool University. His research interests include bioinformatics, deep learning, medical image analysis, and natural language processing.

JIAMING ZHANG received the B.S. degree in communication engineering from Chongqing University, China, in 2007, and the M.S. degree in control systems from the University of Sheffield, U.K., in 2008, and the Ph.D. degree in computer science from the University of Sheffield, in Spring 2013. He joined the Neurocomputing and Robotics Group led by Prof. N. Sharkey and Dr. A. J. C. Sharkey, with the Department of Computer Science, University of Sheffield, in October, 2008. He joined the Advanced Robotics Laboratory (ARL), The Chinese University of Hong Kong, Hong Kong, as a Research Assistant. He is currently a Senior Researcher with the Institute of Robotics and Intelligent Manufacturing, The Chinese University of Hong Kong at Shenzhen, Shenzhen, China. He has also led and participated in more than ten research projects, and has published more than ten research articles and has applied for more than ten patents in the field of robotics and AI. He is a member of Guangdong Association for Artificial Intelligence and Robotics, China. He is also working as a Guest Senior Researcher with the Peng Cheng Laboratory (a National Key Laboratory based in Shenzhen), and with the Shenzhen Institute of Artificial Intelligence and Robotics for Society, China. His research interests include socially interactive robots, health care robotics, marine robotics, pattern recognition and artificial intelligence, deep reinforcement learning, robotic hardware, and smart sensors design.